Impact of environmental noise on oscillatory pattern formation in crystal growth: Plagioclase feldspar

Sergei Katsev and Ivan L'Heureux
Ottawa-Carleton Institute for Physics, University of Ottawa, Ottawa, Ontario, Canada K1N 6N5
(Received 26 October 1999)

Recently, a model for oscillatory zoning in a geochemical system (plagioclase feldspar) was proposed. In that model, oscillations in the composition are generated through a Hopf bifurcation. In this paper, the effects of fluctuations of the bulk composition are studied by means of computer simulations. It is shown that environmental noise can lead to pattern formation such as oscillatory zoning, even when no deterministic periodic solutions exist. The fluctuations in the bulk composition thus lead to an enlargement of the range of system's variables values for which oscillatory zoning occurs. Coherence resonance close to the Hopf bifurcation is also observed in such a system.

PACS number(s): 05.40.−a, 05.45.−a, 05.65.+b, 91.65.−n

I. INTRODUCTION

Many naturally formed minerals exhibit a more or less regular variation of chemical composition from the core of the crystal to its rim. Such patterns are called oscillatory zoning, and are found in a great variety of minerals [1] formed under very different conditions. Oscillatory zoning is observed in crystals from igneous, sedimentary, and metamorphic environments, and in hydrothermal deposits. Probably the oldest known example of this phenomenon is oscillatory zoning in plagioclase feldspar, which is a mineral that is found in many rocks. Oscillatory zoned samples are most common in intermediate composition volcanic rocks [2,3]. In this paper, we investigate the impact of environmental noise on pattern formation in plagioclase.

This mineral is essentially a binary solid solution with two end members: anorthite $CaAl_2Si_2O_8$ (An) and albite $NaAlSi_3O_8$ (Ab). Oscillatory zoned samples show clearly visible patterns, whereby the An concentration varies from the core of the crystal to its rim. Microprobe analysis shows that the An molar composition varies by approximately 5–15 %. Typical samples have tens of zones ranging in thickness from 10 to 100 μm. Superimposed on these more or less regular variations, abrupt changes and irregular patterns are often found [3]. The oscillatory zoned crystals are formed from multiply saturated silicate liquids within magma chambers. The patterns are found frozen into crystals erupted from these chambers as lava flows, or as the eroded remnants of slowly cooled plutonic rocks. The crystallization from the melt typically occurs in far-from-equilibrium conditions, so that kinetic arguments must be used to model the pattern formation.

Holten and co-workers [4,5] suggested that external noise (such as rapid variations of fluid's composition due to magma mixing, gas releases or temperature changes) may play an important role in the formation of the oscillatory patterns in crystals. By studying the effects of environmental noise on a generic crystal-melt system, they showed that fluctuations that occur on scales much larger than the size of the growing crystal produce realistic zoning patterns. In the first work [4], they used a bounded Brownian noise fluctuation superimposed on the bulk composition with a rather long correlation time and large amplitude (about 30% of the average bulk composition). As a consequence, the concentration pattern follows the fluctuations of the bulk concentration. In this case, the diffusive system acts as a filter that eliminates small scale variations. In the second paper [5], four crystal growth models were analyzed for possible noise sensitivity: plagioclase growth in magmatic systems [6], carbonates in sedimentary systems [7], garnets in hydrothermal systems [8], and silicate growth from a melt [9]. In the absence of noise, all these models produce oscillatory or chaotic solutions. It was found that these solutions are sensitive to noise in the boundary condition, the plagioclase model being the most sensitive. In the garnet case, external noise may cause synchronization, so that different crystals develop statistically similar zoning patterns, even if zoning is controlled by local nonlinear processes. This implies that intracrystalline similarity in zonation is not necessarily a direct reflection of gross changes in the external conditions. In all simulations, a bounded Brownian noise with a rather long correlation time was used.

In contrast, our simulations indicate that oscillatory zoning can be caused by uncorrelated noise of small amplitude. In presence of noise, our model produces oscillatory patterns even when no deterministic oscillations exist. The patterns are then formed as a result of the complex interplay between the stochastic external processes and the internal nonlinear dynamics of the system. The external noise thus triggers, rather than drives, the system's dynamics, and noise-induced phenomena, such as coherence resonance and advancement of bifurcation points, are possible.

The paper is organized as follows. First we review the deterministic oscillatory zoning model and introduce its simplified form, which allows a more detailed analysis. Then we discuss the terms that describe the effects of environmental noise. In Sec. IV we present the simulation results and discuss them. Section V describes the Fokker-Planck equation and the analytical method that allows to predict the behavior of systems subjected to noise, as applied to the present study. Finally, we conclude our findings in Sec. VI.

II. MODEL

A. Deterministic growth model

Our model is based on the isothermal nonlinear plagioclase growth model proposed by L'Heureux and Fowler [10,11]. In the rest of this paper, we will refer to this model as the partial differential equation (PDE) model. We assume crystal growth in one dimension, and we choose a frame of reference moving with the interface, so that $x=0$ corresponds to the crystallization front. The dynamical evolution of the concentration of An (mole per unit volume) in the melt $c(x,t)$ is then described by the diffusion equation

$$\frac{\partial c}{\partial t}=\frac{\partial}{\partial x}\left(D\frac{\partial c}{\partial x}\right)+V(c(0,t))\frac{\partial c}{\partial x}, \tag{1}$$

where $c(0,t)$ is the An concentration in the melt near the interface, and D is the effective diffusion coefficient. We neglect the concentration dependence of this coefficient. The growth velocity V is determined only by the local concentration at the interface $c(0,t)$. Since molar volumes of An and Ab are nearly equal, the molar concentration c can be nondimensionalized by the molar volume of An [10]. This way, it becomes equivalent to the molar composition of An in the solution and is bounded $0<c<1$.

A realistic expression for $V(c(0,t))$ for a given temperature T was approximated [10] by fitting the empirical data obtained for synthetic plagioclase [12] to the Calvert-Uhlmann growth model [13]:

$$V=U(R_sR_c^2)^{1/3}. \tag{2}$$

Here the growth is interpreted as a geometric average of two mechanisms, a longitudinal growth R_s by surface nucleation, and a continuous growth R_c along the surface. U denotes a velocity scale. Expressions for R_s and R_c are given by

$$R_s=\exp\left(-\frac{3a}{T\Delta T}\right)\exp\left(-\frac{b}{T-T_g}\right), \tag{3}$$

$$R_c=\left[1-\exp\left(-\frac{\Delta G}{RT}\right)\right]\exp\left(-\frac{b}{T-T_g}\right). \tag{4}$$

Here the parameter a is related to the surface tension of the critical nucleus, b to the viscosity of the melt, and $\Delta T=T_L-T$ is the undercooling, with T_L being the liquidus temperature and T_g the glass-transition temperature. ΔG is the difference in molar Gibbs free energy between the crystal and the melt. The concentration dependence of the growth velocity comes mainly from the liquidus line $T_L(c(0,t))$ and the velocity scale $U(c(0,t))$ [10].

The boundary condition far from the crystal-melt interface is such that the concentration is equal to the bulk concentration of An in the melt:

$$c(\infty,t)=\hat{c}. \tag{5}$$

The boundary condition at the growing front is derived from the continuity of mass flux at the crystal interface:

$$D\left.\frac{\partial c}{\partial x}\right|_{x=0}+[c(0,t)-c_s(t)]V=0. \tag{6}$$

Here $c_s(t)$ is the interface An concentration in the crystal. We have neglected the diffusion in the solid phase. A nonlinear phenomenological partitioning relation between $c_s(t)$ and $c(0,t)$ was proposed by Lasaga [14]:

$$c_s(t)=\frac{K_DBc(0,t)}{A+(K_D-1)c(0,t)}. \tag{7}$$

If c' refers to the concentration of another major component (i.e., Ab) in the solution, then $K_D=c_s(t)c'(0,t)/[c(0,t)c_s'(t)]$ is an effective exchange-equilibrium constant whereas $A=c(0,t)+c'(0,t)$ and $B=c_s(t)+c_s'(t)$ are approximately constants [14]. When c refers to the concentration of a trace element, a simple relation can also be used that employs a constant partitioning coefficient K:

$$c_s(t)=Kc(0,t). \tag{8}$$

The nonlinear relation (7) reduces to Eq. (8) if we assume $c\approx$const in the denominator of Eq. (7). For simplicity, expression (8) is used in the reduced model described below. The nonlinear coupling necessary to generate self-oscillatory solutions is generated by the nonlinear concentration dependence of the growth velocity V.

In conditions close to equilibrium, the partitioning coefficients K_D or K can be derived from the equilibrium phase diagram, and are larger than unity. However, in situations where far-from-equilibrium conditions prevail, K_D or K must be derived from kinetic arguments [9] and can take values smaller than 1.

In the model [Eqs. (1)—(7)], a steady state solution for c_s exists. For $K_D>1$, this steady state solution is stable and the system relaxes to this fixed point without oscillations. This corresponds to the situation where the crystal has a constant, well defined An composition, as is observed in crystals formed in close-to-equilibrium conditions. For $K_D<1$ there is a regime where underdamped oscillations to the steady state exist. For smaller values of K_D, the system undergoes a Hopf bifurcation, beyond which the attractor is a limit cycle. For a typical value of $\hat{c}=0.3$ at $T=1400\,^\circ$C, the Hopf bifurcation occurs at $K_D=0.24$ [11]. A transition to chaotic behavior through a period doubling sequence is also observed for still smaller values of K_D. The simpler form [Eq. (8)] of the partitioning relation (7) produces similar sequences of dynamical behavior: as K decreases, there is a transition from steady state to a limit cycle through a Hopf bifurcation and then to chaos [10].

B. Reduction to two nodes

The description of the diffusion process can be simplified by rewriting the model in terms of ordinary differential equations. Wang and Merino [15] proposed a dynamical model of zoning in calcite and plagioclase, which is based on the evolution of the concentration of two compounds at one point near the interface. This results in two coupled ordinary differential equations, which can generate oscillatory solutions. Here we adopt the spirit of their approximations, and take the idea one step further by suggesting a reduction of the crystallization dynamics to the concentration evolution at two distances L_1 and L_1+L_2 from the growth front (Fig. 1). This

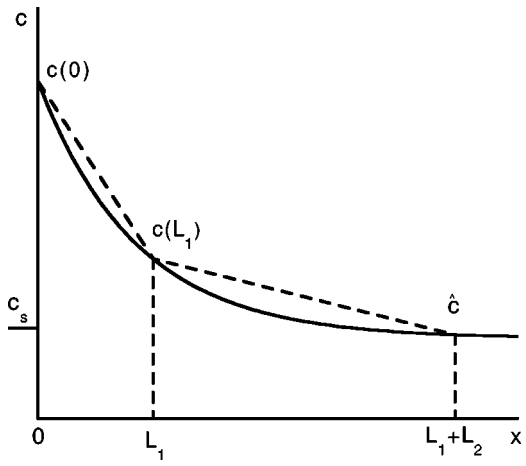

FIG. 1. Reduction of the plagioclase growth-transport processes to the An concentration evaluated at two nodes: at the interface, and at the distance L_1 from the interface. The smooth concentration profile is approximated by linear segments. The concentration at the distance L_1+L_2 is taken to be equal to the bulk concentration of An, $\hat{c}$. The An concentration in the crystal c_s is related to the concentration in the melt at the interface $c(0)$ through the partitioning relation (8).

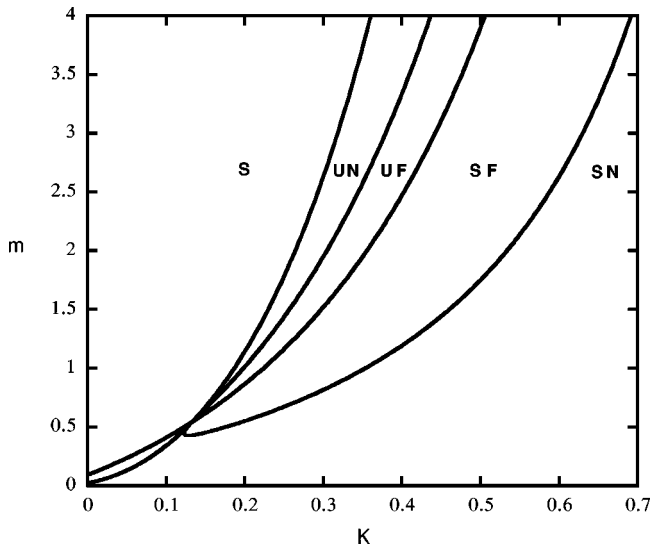

FIG. 2. Stability diagram for the global fixed point in the two-node model described by Eqs. (13) and (14). The stability regions are as follows: S, saddle; UN, unstable node; UF, unstable focus; SF, stable focus; SN, stable node. The parameters are $l=0.25$ and $d=0.5$.

enables us to describe the essentially continuous process by two coupled ordinary differential equations that mimic the general dynamics of the parent model and allow for the possibility of a limit cycle. A stability analysis can be easily performed as well. We will refer to this approximation as the two-node model, from the nomenclature conventionally used in finite element techniques.

We integrate the diffusion equation (1) with respect to the space coordinate, and take the following approximations [15] (see Fig. 1):

$$\int_0^{L_1} c\,dx=[c(L_1)+c(0)]L_1/2, \tag{9}$$

$$\left.\frac{\partial c}{\partial x}\right|_{0<x\leq L_1}=[c(L_1)-c(0)]/L_1. \tag{10}$$

Similarly,

$$\int_{L_1}^{L_1+L_2} c\,dx=[c(L_1+L_2)+c(L_1)]L_2/2, \tag{11}$$

$$\left.\frac{\partial c}{\partial x}\right|_{L_1<x\leq L_1+L_2}=[c(L_1+L_2)-c(L_1)]/L_2. \tag{12}$$

The boundary condition (5) becomes $c(L_1+L_2)=\hat{c}$. After imposing condition (6) and taking into account the partition relation (8), we obtain the following system of two ordinary differential equations:

$$\dot{\alpha}\equiv f_1(\alpha,\beta)=d\beta(1+l+l^2)-d\alpha(1+l)-dl^2-v(\alpha)K\alpha + v(\alpha)\beta(1+l)-v(\alpha)l, \tag{13}$$

$$\dot{\beta}\equiv f_2(\alpha,\beta)=dl^2-d\beta l(1+l)+dl\alpha+v(\alpha)l-v(\alpha)l\beta. \tag{14}$$

Here the dimensionless variables are $\alpha=c(0)/\hat{c}$, $\beta=c(L_1)/\hat{c}$, $l=L_1/L_2$, $v(\alpha)=V/V_0$, and $d=D/(V_0L_1)$, and the dimensionless time is $\tau=2tV_0/L_1$. We have introduced V_0 as a typical growth velocity scale; for instance, the value corresponding to the steady growth regime. We approximate the crystal growth velocity as

$$V(\alpha)=V_0\exp[m(\alpha-\alpha_{st})], \tag{15}$$

where α_{st} is the concentration in the melt in the steady growth regime and m is a constant. Equation (15) is a fairly good approximation of the experimental data [12] for a wide range of temperatures if $\hat{c}$ is large enough (e.g., $\hat{c}>0.2$, and for a typical growth temperature $T=1400\,^{\circ}\mathrm{C}$ [10]). For $T=1400\,^{\circ}\mathrm{C}$ the corresponding value of the factor m is 2.96.

C. Stability analysis

For all values of the parameters in the two-node model [Eqs. (13) and (14)], there exists at least one fixed point, which we will call ''global.'' By definition, we choose a velocity scale such that $V=V_0$ at this point for all parameter values. A stability diagram for this fixed point is shown in Fig. 2. Similarly to the full plagioclase growth model [Eqs. (1)–(7)], for $K>1$ the fixed point is always a stable node. As K decreases, the fixed point changes to a stable focus and then to an unstable focus through a Hopf bifurcation. For reasonable values of the parameters $m=2.96$, $l=0.25$, and $d=0.5$ the Hopf bifurcation generates a stable limit cycle at $K=0.439$. For $K<0.426$, two new fixed points are created through a tangent bifurcation: a saddle point and a stable node. The limit cycle solution then loses its stability. Since the Hopf bifurcation occurs at a value of K higher than in the PDE model, we do not expect quantitative agreement between the two models. However, the dynamics are analogous in the neighborhood of the Hopf bifurcation. For our purpose of investigating how external noise can influence the genera-

tion of periodic solutions, the most interesting region is the one close to the Hopf bifurcation, where the global fixed point is a stable focus.

III. STOCHASTIC ENVIRONMENTAL FLUCTUATIONS

Suppose the system is subjected to some environmental noise such as fluctuations of temperature or concentrations of elements. Since changes in the system's parameters can be caused by a variety of different factors (e.g., gas releases, magma mixing, etc.), it is reasonable to assume that the amplitude of the fluctuations would follow a Gaussian distribution. We also postulate that these changes occur over a time scale which is much faster than the crystal growth time, and can be considered uncorrelated. Therefore, we choose white Gaussian noise as an approximation for the environmental fluctuations. Plagioclase crystals grow in an environment where thermal diffusivity is much greater than component diffusion. Consequently, the process is mostly isothermal [16]. We will investigate the effects of fluctuations in the bulk concentration $\hat{c}$ of the element in a fashion similar to Holten *et al.* [4].

In the full growth model described by the PDE (1), the noise would appear in the modified boundary condition (5),

$$c(\infty,t)=\hat{c}[1+\sigma\xi(t)], \tag{16}$$

where σ denotes the amplitude of the noise relative to $\hat{c}$, and $\xi(t)$ is a Gaussian white process with zero mean:

$$\langle\xi(t)\rangle=0, \tag{17}$$

$$\langle\xi(t)\xi(t')\rangle=2\delta(t-t'). \tag{18}$$

In the reduced two-node model [Eq. (13)], fluctuations of the form $c(L_1+L_2,t)=\hat{c}[1+\sigma\xi(t)]$ lead to multiplicative noise terms

$$\dot{\alpha}=f_1(\alpha,\beta)-(dl^2+vl)\sigma\xi(t), \tag{19}$$

$$\dot{\beta}=f_2(\alpha,\beta)+(dl^2+vl)\sigma\xi(t), \tag{20}$$

where f_1 and f_2 are the right hand sides of Eq. (13). We have disregarded the terms that contain the time derivative of the noise. These terms become important when the correlation time of the noise approaches zero. However, preliminary simulations, in which the algorithm of Ref. [17] for an Ornstein-Uhlenbeck colored noise was used, indicate that there is a wide range of noise correlation times for which the approximation (19) is valid. In this range the correlation time of the noise is large enough so that the derivative terms are negligible, and at the same time it is much smaller than the dynamical time scale of the deterministic system so that the white noise approximation is still useful. It should be noted that, although the terms that contain the time derivative of the noise have no physical meaning in the case of white noise, they may play a significant role in the dynamics of the system in the case of colored noise (e.g., it may shift the bifurcation point from its deterministic value [18]). A detailed analysis of the effect of noise color is under investigation.

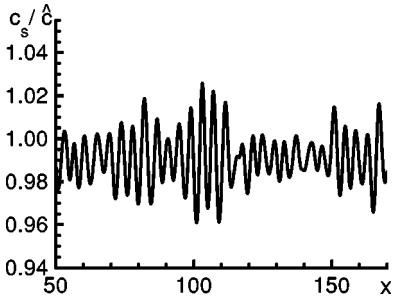

FIG. 3. Spatial concentration profile generated by the full PDE model. $T=1400\,^{\circ}\mathrm{C}$, $\hat{c}=0.3$, $K=0.25$, and $\sigma=5\times10^{-3}$. The deterministic attractor for these parameter values is a stable focus. The transient solution is not shown. One space unit corresponds to 6.62 μm.

IV. RESULTS AND DISCUSSION

Concentration profiles were generated in two ways. The partial differential equation (1) was solved using a Crank-Nicholson finite difference scheme with iteration of the nonlinear terms. The ordinary stochastic differential equations (19) and (20), were integrated using the first order method adapted from Ref. [17], which turned out to be sufficiently precise for our purposes. The Stratonovich interpretation of this algorithm was employed. Other algorithms such as Heun's [19] yield similar results. To obtain results analogous to direct observations, we need to produce the spatial profile of the concentration in the crystal. In order to do so, the space coordinate was obtained by integration [10,11]:

$$x(t)=\int_0^t v(\alpha(t'))dt'. \tag{21}$$

Transformation of the time series into spatial profiles generally biases the shape of the concentration spikes toward the crystallization front.

We investigated the system's response to external noise in the region of the parameter space that corresponds to the deterministically stable fixed point close to the Hopf bifurcation. Typical crystal concentration profiles simulated according to the PDE and the two-node models, respectively, are shown in Figs. 3 and 4. The simulation results show that the generated patterns exhibit an oscillatory behavior. Thus

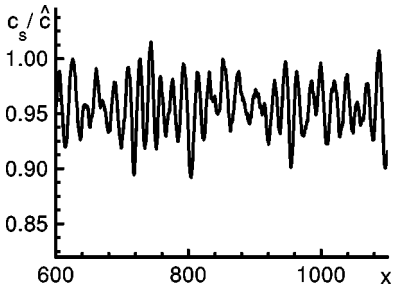

FIG. 4. Spatial concentration profile generated by the two-node model. $K=0.445$, $m=2.96$, $l=0.25$, $d=0.5$, $\hat{c}=0.3$, and $\sigma=10^{-4}$. The deterministic attractor for these parameter values is a stable focus. The transient solution is not shown. One space unit corresponds to 21.79 μm.

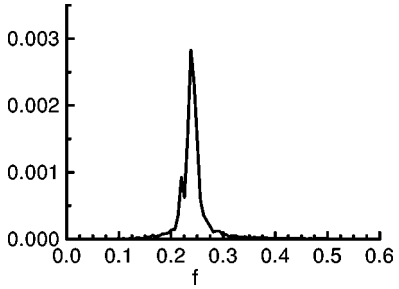

FIG. 5. Power spectrum computed from the time series corresponding to the space concentration profile shown in Fig. 3. One frequency unit corresponds to 0.228 Hz.

oscillatory concentration patterns are possible in the presence of noise even when no oscillation exists deterministically.

The amplitude of the stochastic oscillations of the crystal An concentration derived from the PDE model is about 2% for a noise amplitude of 5×10^{-3}. This is of the same order of magnitude as the lower limit of observed concentration variations. In Fig. 3, the average zone width is 27μm.

Replacing the exponential diffusion profile of concentration by linear segments (Fig. 1) makes the interface composition more susceptible to the fluctuations of the bulk concentration. The two-node model thus possesses a slightly greater sensitivity to the external noise. Changes in crystal An concentration of the same magnitude (2%) are generated by a noise amplitude of only 10^{-5}. In Fig. 4, the average zone width is 416 μm, which is large compared to actual zone widths. However, as mentioned earlier, quantitative agreement is not expected from this simplified model. Nevertheless, both the full and reduced models exhibit similar qualitative dynamics in terms of the shape of the concentration profiles.

A spectral analysis was performed on the time series. Close to the Hopf bifurcation, the frequency of the motion around the stable focus manifests itself in the dynamics of the noise-perturbed system. While the spectrum of the external noise is flat, the characteristic peak of the system's natural frequency is clearly visible in the power spectrum (Figs. 5 and 6). The amplitude of the oscillations increases as the noise amplitude increases. As the parameter K increases, thus taking the system away from the Hopf bifurcation, the oscillations become smaller in amplitude, and additional frequencies become more noticeable.

In general, before the Hopf bifurcation point, an increase in the noise intensity may have two general effects on the power spectrum of the response [20]. First, due to the nonlinearity of the system, the quality factor of the oscillator deteriorates, and consequently the spectral peak may become broader. This effect was found to be insignificant in the present case. The width of the peak remained approximately constant over a wide range of noise intensities. Second, as the noise kicks the system's trajectory farther from its stable point, the amplitude of the damped oscillation becomes larger, thus increasing the height of the peak in the power spectrum. The exact dependence of the peak height on the intensity of external perturbations is determined by the system's nonlinearity, and may be partly controlled by noise. The strength of the response increases with the amplitude of the noise but is limited by the system's nonlinearity. As a result, the system's response is maximized for a certain noise amplitude.

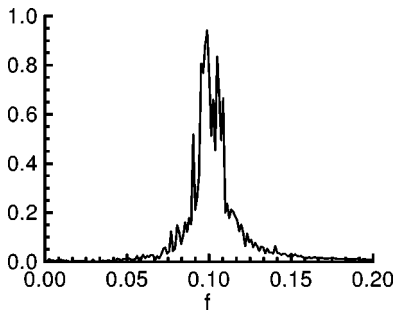

FIG. 6. Power spectrum computed from the time series corresponding to the space concentration profile shown in Fig. 4. One frequency unit corresponds to 0.019 Hz.

The strength of the system's response to the external noise can be quantified by R, the signal-to-noise ratio (SNR). While several definitions of the SNR are used in characterizing the behavior of a noisy system near the bifurcation [20,21], we choose the one that is best suited to describe our system's response around a frequency of interest relative to the broad-spectrum response around this frequency. Thus we define the SNR at some particular frequency Ω as the ratio of the area of the peak to the characteristic value of the background spectral response at this frequency [22]:

$$R=\left[\int_{\Omega-\Delta\omega_1}^{\Omega+\Delta\omega_2} S(\omega)d\omega\right]/S_b(\Omega). \tag{22}$$

Here $\Delta\omega_1+\Delta\omega_2$ defines the width of the integration window around Ω, and $S_b(\Omega)$ is the value of the floor line at the frequency of interest. The floor line is drawn to join the boundaries of the peak defined by the integration window. The function $S(\omega)$ is a Fourier transform of the correlation function:

$$S(\omega)=\hat{c}^{-2}\int_{-\infty}^{+\infty} e^{-i\omega\tau}\langle\langle c_s(t+\tau)c_s(t)\rangle\rangle d\tau. \tag{23}$$

The double bracket indicates that the correlation function is averaged over the realizations of the noise as well as over the phase of the deterministic damped oscillations that exist in the region where the fixed point is a stable focus.

The SNR's obtained from both models have a distinct peak (Figs. 7 and 8). The system's response to the external noise shows a steep increase in the range of small noise intensities. As the noise increases, the SNR slowly decreases.

The response of the system to noise indicates that a so called noisy precursor of the bifurcation [23] is observed in the vicinity of the Hopf bifurcation. In general, before the Hopf bifurcation, the power spectrum will have a strong response at a frequency close to that of the limit cycle created at the bifurcation point. The fact that the SNR curve passes through a maximum suggests that there is a so called coherence resonance (CR) [20], i.e., the response of a nonlinear system to noise is optimized for a certain noise amplitude. Coherence resonance, also often called autonomous or internal stochastic resonance, occurs in nonlinear oscillating sys-

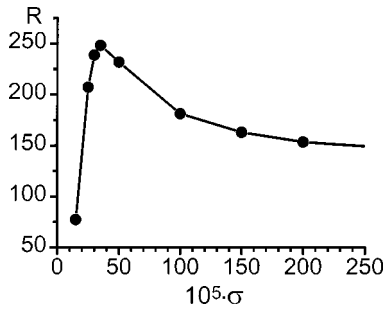

FIG. 7. Signal-to-noise ratio computed from the PDE model. $T=1400\,^{\circ}\mathrm{C}$, $\hat{c}=0.3$, and $K=0.25$. The deterministic attractor for these parameter values is a stable focus. The spectral response is averaged over 400 noise realizations as well as over the phase of the deterministic damped oscillations. The window of integration in Eq. (22) contained 14 bins.

tems, whose internal dynamics depends on the noise amplitude. As pointed out [20], the behavior of the SNR in CR is often very similar to that of stochastic resonance (SR). The phenomenon of SR typically occurs in periodically driven stochastic bistable systems, and has been the object of various studies in the past decade (for a review, see Ref. [22]). The resonancelike amplification of a weak external signal occurs when its frequency matches the characteristic rate of stochastic hopping between the two states. In SR, the SNR as a function of the noise amplitude is a curve with a well-defined maximum. Coherent resonance is said to occur when the noise stimulates a coherent motion in an autonomous system (i.e., without external signal).

Along with the main frequency, several lower frequencies consistently appear near the main peak, and become more apparent as the system moves farther from the bifurcation in the stable region. One of them, located close to the main frequency, causes a beatlike pattern in the concentration profiles (Fig. 3).

It is interesting to note that even for values of $K>1$, when no damped deterministic oscillation exists, the external noise has some organizing influence on the crystallization process (Fig. 9). Here small variations of concentration form a correlated pattern that is very different from the input uncorrelated noise (in contrast to the case studied by Holten *et al.* [4]).

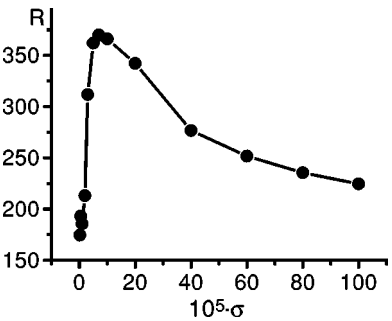

FIG. 8. Signal-to-noise ratio computed from the two-node model. $K=0.445$, $m=2.96$, $l=0.25$, and $d=0.5$. The deterministic attractor for these parameter values is a stable focus. The spectral response is averaged over 1000 noise realizations as well as over the phase of the deterministic damped oscillations. The window of integration in Eq. (22) contained 32 bins.

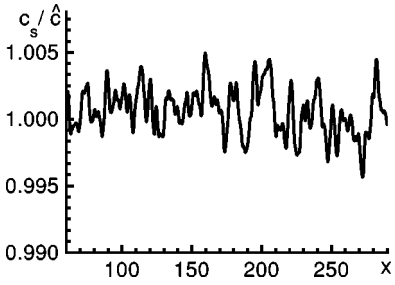

FIG. 9. Spatial concentration profile generated by the PDE model. $T=1400\,^{\circ}\mathrm{C}$, $\hat{c}=0.3$, $K=1.20$, $\sigma=5\times10^{-3}$. The deterministic solution for these parameter values is a stable node. The transient solution is not shown. One space unit corresponds to 210 μm. Variations occur on a much larger horizontal scale than in the case of smaller K because of the strong dependence of the steady state velocity scale to the value of K.

Figure 10 shows a return map for the PDE model, i.e., the width W_{n+1} of the $(n+1)$th zone plotted versus the width W_n of the nth zone in Fig. 3. This type of analysis is common in nonlinear dynamics to identify what might be a low dimensional chaotic attractor. Since random noise is a key part of our models, there should be no particular pattern for small noise intensities. Indeed, in the low noise range the points seem to fill up the space evenly, which is a signature of randomness. When the noise takes the system far enough from its steady state, the deterministic dynamics of the system prevails over the stochastic motion. For large excursions the return map seems to exhibit a triangular pattern similar to the one observed for natural plagioclase [24]. The emergence of such a pattern may indicate a possibility of noise-induced chaos. The return maps obtained from the reduced two-node model show no sign of such a pattern (Fig. 11). This can be expected because the triangular nonrepeating pattern may be a signature of chaotic attractor while the dimension of model (13) does not allow for chaotic solutions. The idea that zoning in plagioclase could be a result of a complex interplay between the deterministic nearly oscillatory internal dynamics and the external stochastic fluctuations is supported by the fact that in many cases the return maps for plagioclase appear random, and no specific fractal dimension can be found [4].

V. FOKKER-PLANCK EQUATION

Given the Langevin type equations (13) and (14), we can obtain a corresponding equation describing the evolution of

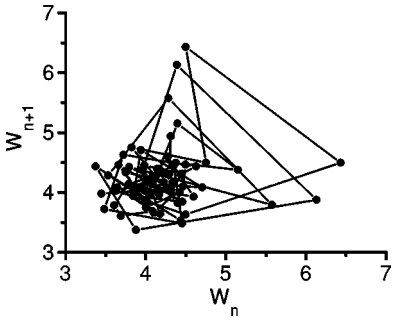

FIG. 10. Return map corresponding to the space concentration profile generated by the full PDE model of Fig. 3. One space unit corresponds to 6.62 μm.

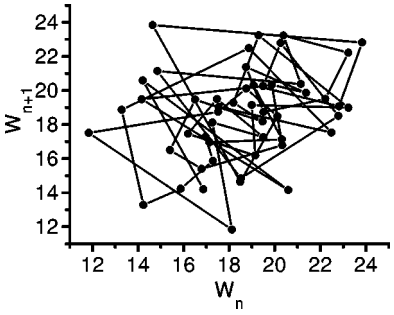

FIG. 11. Return map corresponding to the space concentration profile generated by the two node model of Fig. 4. One space unit corresponds to 21.79 μm.

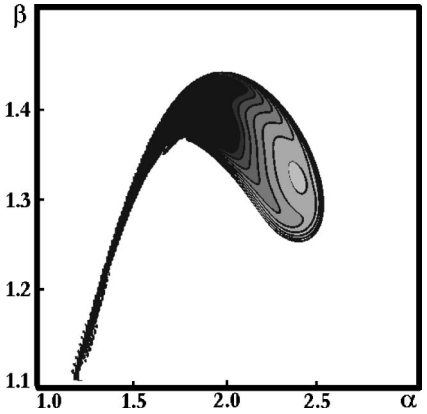

FIG. 12. Logarithm of the stationary probability density obtained as a solution of the Fokker-Planck equation (24) corresponding to the 2-nodes model. $K=0.445$, $d=0.5$, $m=2.96$, $\sigma=0.02$, and $\hat{c}=0.3$. The deterministic attractor for these parameter values is a stable focus located at $\alpha=2.15$, and $\beta=1.35$. Darker areas correspond to higher probability densities. The spacing between level curves is 0.2 and the value of $\ln p$ corresponding to the light level curve in the crater is -0.3. The presence of a crater suggests the existence of a limit cycle and, consequently, a shift in the Hopf bifurcation point (advancement). The ''tail'' represents a slow manifold, which is responsible for the appearance of sawtooth patterns in the spatial concentration profiles at higher noise intensities.

the probability density of finding the system in a certain region of parameter space [25]. This equation allows visualization of the shape of the probability density, to investigate the possibilities of noise-induced states and shifts in the deterministic bifurcation points as the system parameters change. In the case of white noise, this equation [the Fokker-Planck equation (FPE)] is easily derived and can be solved exactly for univariate systems. In most multivariate systems, the FPE must be solved numerically.

The FPE for the two-node model [Eqs. (19) and (20)] can be written in the Stratonovich interpretation as

$$\frac{\partial p}{\partial \tau} = -p\left(\frac{\partial f_1}{\partial \alpha}+\frac{\partial f_2}{\partial \beta}\right)-f_1\frac{\partial p}{\partial \alpha}-f_2\frac{\partial p}{\partial \beta} + \frac{\sigma^2}{2}\left[g^2\left(\frac{\partial^2 p}{\partial \alpha^2}+\frac{\partial p}{\partial^2 \beta^2}-2\frac{\partial^2 p}{\partial \alpha \partial \beta}\right) + 3gg'\left(\frac{\partial p}{\partial \alpha}-\frac{\partial p}{\partial \beta}\right)+p(g'^2+gg'')\right], \qquad (24)$$

where $p=p(\alpha,\beta,\tau)$ is the probability density of the system to be in a state around (α,β) at time τ, $f_1=f_1(\alpha,\beta)$ and $f_2=f_2(\alpha,\beta)$ are the deterministic terms defined in Eqs. (13) and (14), $g=g(\alpha)=-[dl^2+v(\alpha)l]$ is the multiplicative part of the stochastic term in Eqs. (19) and (20), and σ is the intensity of the noise. In the stationary regime ($\partial p/\partial \tau=0$), the boundary conditions are naturally defined as the absence of probability flux across the borders of the region $0<\{\alpha,\beta\}<1/\hat{c}$.

The stationary version of Eq. (24) was solved numerically using the successive overrelaxation method. Figure 12 shows the stationary probability distribution corresponding to the regime for which the stable focus exists before the Hopf bifurcation ($K=0.445$, $\sigma=0.02$). The coordinates are the dimensionless An concentrations α and β in the melt near the interface and at the distance L_1 from it, respectively. The maximum of the probability density is shifted from the deterministic fixed point. A small crater is formed, which suggests the presence of a stochastic limit cycle, and consequently a noise-induced shift in the bifurcation point (advancement). A distinct feature is the presence of a tail-shaped slow manifold adjacent to the area around the deterministic fixed point. The maximum of the probability density is located on this manifold. In terms of the system's dynamics, any relatively large fluctuation in the concentration makes the system converge to this manifold very quickly. After that, it takes a long time to come back to the vicinity of the stable focus. This results in a sawtooth shape of the concentration time series and space profiles at high noise intensities.

The question arises whether the noise truly advances the Hopf bifurcation point. In a ''naive'' generic case, based on the normal form for the Hopf bifurcation, postponement of the bifurcation is expected. However, it was shown [18] for the Brusselator system (an important example exhibiting a Hopf bifurcation) that multiplicative noise coupled to a fast variable may cause an advancement of the bifurcation point. Although for this particular case, analog simulations [26] found only postponements, some qualitative agreement with the prediction of Ref. [18] in terms of shifts in the probability density was observed. In our model, the system's motion is faster in a direction approximately perpendicular to the tail-shaped slow manifold of Fig. 12. From Eqs. (19) and (20), it is seen that the variable $\alpha+\beta$ is deterministic. Therefore, the noise effectively drives the system in the direction $\beta=-\alpha$, which approximately corresponds to the direction of the fast motion. This provides a coupling mechanism between the noise and a fast variable in analogy with the Brusselator case [18]. Whether we can analytically prove advancement of the Hopf bifurcation in the present case, as it is suggested by our numerical results, is currently the subject of further studies.

VI. CONCLUSION

We have shown that fluctuations of environmental parameters can lead to pattern formation exhibiting an oscillatory character in plagioclase. Such fluctuations may supposedly

be caused by magma mixing, changes in H_2O content, releases of gases, or temperature variations. The exact physical nature of these environmental fluctuations as well as their magnitude is an interesting question but outside the scope of the present work.

In our model of plagioclase growth from melt, relatively small random fluctuations of the bulk concentration of An stimulate the internal dynamical processes, which result in a more or less regular zoning. Close to a Hopf bifurcation, the noise causes oscillations with a frequency close to the frequency that the system would have after the bifurcation. As a side effect, some lower frequencies are also generated. The signal-to-noise ratio exhibits a distinct peak typical of coherence resonance phenomena. The effect of noise thus extends the available parameter space for which oscillatory zoning may be observed.

The return maps generated according to the full stochastic PDE model for large excursions show a triangular pattern similar to the one observed in natural plagioclase. The reduced two-node model, in which the spatial dependence of the concentration is approximated by straight lines, has a dynamical behavior which is similar to the full PDE model around the Hopf bifurcation point. Solution of the Fokker-Planck equation for this case suggests the possibility of advancement of the bifurcation due to noise.

The presence of a slow manifold in the region of phase space adjacent to the area around the deterministic fixed point results in oscillations taking the form of spikes. Since the model is described by two variables, it is unable to produce chaotic deterministic solutions. As a next step, one could suggest a three-node reduction that would then allow one to simulate the chaotic behavior.

ACKNOWLEDGMENTS

The authors would like to thank the Natural Sciences and Engineering Research Council of Canada for financial support, and Anthony Fowler, André Longtin, and Bjørn Jamtveit for fruitful discussions.

[1] M. Shore and A. D. Fowler, Can. Mineral. **34**, 1111 (1996).
[2] T. Pearce, in *Feldspars and Their Reactions*, Vol. 421 of *NATO Advanced Study Institute, Series C: Mathematical and Physical Sciences*, edited by I. Parsons (Kluwer Academic, Dordrecht, 1994), pp. 313–346.
[3] T. H. Pearce and A. M. Kolisnik, Earth-Sci. Rev. **29**, 9 (1990).
[4] T. Holten, B. Jamtveit, P. Meakin, M. Cortini, J. Blundy, and H. Austrheim, Am. Mineral. **82**, 596 (1997).
[5] T. Holten, B. Jamtveit, and P. Meakin, Geochim. Cosmochim. Acta. (to be published).
[6] I. L'Heureux and A. D. Fowler, Can. Mineral. **34**, 1137 (1996).
[7] Y. Wang and E. Merino, Geochim. Cosmochim. Acta **56**, 587 (1992).
[8] B. Jamtveit, Am. Mineral. **76**, 1319 (1991).
[9] J.-H. Wang and J.-P. Wu, Eur. J. Mineral. **7**, 1089 (1995).
[10] I. L'Heureux, Phys. Rev. E **48**, 4460 (1993).
[11] I. L'Heureux and A. D. Fowler, Geophys. Res. Lett. **23**, 17 (1996).
[12] R. J. Kirkpatrick, L. Klein, D. R. Uhlmann, and J. F. Hays, J. Geophys. Res. **84**, 3671 (1979).
[13] P. Calvert and D. Uhlmann, J. Geophys. Res. **12**, 291 (1972).
[14] A. Lasaga, Am. J. Sci. **282**, 1264 (1982).
[15] Y. Wang and E. Merino, Am. J. Sci. **295**, 49 (1995).
[16] I. L'Heureux, Physica A **239**, 137 (1997).
[17] M. Sancho, M. San Miguel, S. L. Katz, and J. D. Gunton, Phys. Rev. A **26**, 1589 (1982).
[18] R. Lefever and J. W. Turner, Phys. Rev. Lett. **56**, 1631 (1986).
[19] A. Greiner, W. Strittmatter, and J. Honerkamp, J. Stat. Phys. **51**, 95 (1988).
[20] A. Neiman, P. I. Saparin, and L. Stone, Phys. Rev. E **56**, 270 (1997).
[21] A. Longtin, Phys. Rev. E **55**, 868 (1997).
[22] L Gammaitoni, P. Hngii, P. Jung, and F. Marchesoni, Rev. Mod. Phys. **70**, 223 (1998).
[23] K. Wiesenfeld, J. Stat. Phys. **38**, 1071 (1985).
[24] S. L. Higman and T. H. Pearce, Geophys. Res. Lett. **20**, 1935 (1993).
[25] W. Horsthemke and R. Lefever, *Noise-Induced Transitions. Theory and Applications in Physics, Chemistry, and Biology* (Springer-Verlag, New York, 1984).
[26] L. Fronzoni, R. Mannella, P. V. E. McClintock, and F. Moss, Phys. Rev. A **36**, 834 (1987).